ELECTRON ACCELERATION AND SYNCHROTRON RADIATION IN DECELERATING PLASMOIDS

Charles D. Dermer and James Chiang

E. O. Hulburt Center for Space Research, Code 7653, Naval Research Laboratory, Washington, DC 20375-5352

ABSTRACT

An equation is derived to calculate the dynamics of relativistic magnetized plasma which decelerates by sweeping up matter from the ISM. Reduction to the non-radiative and radiative regimes is demonstrated for the general case of a collimated plasmoid whose area increases as a power of distance x from the explosion, and in the specific case of a blast-wave geometry where the area increases quadratically with x. An equation for the evolution of the electron momentum distribution function in the comoving fluid frame is used to calculate the observed synchrotron radiation spectrum. The central uncertainty involves the mechanism for transfering energy from the nonthermal protons to the electrons. The simplest prescription is to assume that a fixed fraction of the comoving proton power is instantaneously transformed into a power-law, "shock"-like electron distribution function. This permits an analytic solution for the case of a relativistic plasmoid with a constant internal magnetic field. Effects of parameter changes are presented. Breaks in the temporal behavior of the primary burst emission and long wavelength afterglows occur on two time scales for external ISM density distributions $n_{\rm ext} \propto x^{-\eta}$. The first, as emphasized by Mészáros & Rees, represents the time when the outflow sweeps up $\approx \mathcal{M}_{\rm th}/\Gamma_0$ of material from the ISM, where $\mathcal{M}_{\rm th}$ is the mass in the outflow ejecta and Γ_0 is the initial Lorentz factor of the plasmoid. The second represents the time when synchrotron cooling begins strongly to regulate the number of nonthemal electrons that are producing radiation which is observed at a given energy.

Results are applied to GRB and blazar variability. The slopes of the time profiles of the X-ray and optical light cuves of the afterglows of GRB 970228 and GRB 970508 are explained by injection of hard electron spectra with indices $s < 2$ in a deceleration regime near the radiative limit. We also propose that blazar flares are due to the transformation of the directed kinetic energy of the plasmoid when interacting with the external medium, as would occur if relativistic outflows pass through clouds orbiting the central supermassive black hole.

Subject headings: galaxies: active — galaxies: jets — gamma-ray bursts — gamma rays: theory — radiation mechanisms: nonthermal

1. Introduction

CGRO BATSE and *Beppo-SAX* observations of GRBs have renewed interest in relativistic blast-wave models. The BATSE observations (Meegan et al. 1992; Fishman & Meegan 1995) indicate that GRBs originate from cosmological distances and therefore involve impulsive releases of energy exceeding 10^{51} ergs (assuming isotropic emission). The *Beppo-SAX* observations of X-ray afterglows from GRB 970228 (Costa et al. 1997) and GRB 970508 (Piro et al. 1997) led to the first optical counterpart identifications of GRB

sources (van Paradijs et al. 1997; Djorgovski et al. 1997), culminating in the detection of absorption lines from the optical counterpart to GRB 970508, showing that it lies at redshift $z \geq 0.835$ (Metzger et al. 1997). The X-ray emission from GRB 970228 decays as a power-law $\propto t_{\mathrm{obs}}^{-1.33\pm0.12}$ between ≈ 50 s and one week following the GRB (Costa et al. 1997), where t_{obs} is the observer time. The optical counterpart of GRB 970228 decays $\propto t_{\mathrm{obs}}^{-1.12\pm0.08}$ between 0.6 days and 189 days following the burst, though it exhibits apparent fluctuations from a simple power-law (Galama et al. 1997; Garcia et al. 1997).

The X-ray afterglow of GRB 970508 displays a peak at about 2 days following the burst, with an underlying power law decline $\propto t_{\mathrm{obs}}^{-1.1}$ from the end of the main phase of the burst at about 30 sec to ≈ 6.1 days following the GRB (Piro et al. 1997). The optical flux of GRB 970508 appears to be roughly constant between ≈ 6 hrs and 1 day, whereupon it subsequently rises and likewise peaks at ≈ 2 days after the burst (Djorgovski et al. 1997; Sahu et al. 1997 and references therein). The optical emission thereafter declines $\propto t_{\mathrm{obs}}^{-1.18\pm0.04}$ (Garcia et al. 1997). The 4.86 GHz radio emission from GRB 970508 was first detected ≈ 6 days after the GRB, is rapidly variable (evidently due to interstellar scintillation; Goodman 1997) though with an overall flat time profile until ≈ 60 days following the burst, after which it begins to monotonically decline (Frail et al. 1997).

Because of these observations, much interest has been focused on the hydrodynamical study of relativistic blast waves by Blandford & McKee (1976), which has been applied to GRBs by Rees, Mészáros, & coworkers in a series of papers (e.g., Mészáros & Rees 1993, 1997; Mészáros, Rees, & Papathanassiou 1994; Wijers, Rees, & Mészáros 1997; Panaitescu & Mészáros 1997) devoted to understanding the prompt GRB emision and the long wavelength afterglows. Vietri (1997a,b) used the results of Blandford & McKee in the radiative regime to explain the delayed X-rays, and Waxman (1997a,b) applied the blast wave model to the long wavelength afterglows. Mészáros, Rees, & Wijers (1997) have derived power-law time profiles for delayed emission in different regimes assuming analytic models for the ISM density distribution.

Here we reframe the hydrodynamical approach by deriving an equation for plasmoid dynamics in terms of the comoving particle distribution functions. This permits the radiation physics to be treated in the comoving frame, and the plasmoid dynamics to be calculated self-consistently. This approach can be applied, with appropriate modifications, to temporal studies of blazar emissions which are also thought to result from relativistic plasma outflows. Blazar flares, which vary on time scales as short as hours to days in the 1 MeV - 1 TeV regime (e.g., Michelson et al. 1994; Catanese et al. 1997), are in this picture due to the reconversion of directed kinetic energy of the outflowing plasmoid by interactions with the ISM (see Hartman et al. 1997 and Shrader & Wehrle 1997 for recent reviews of blazar observations). We suggest that the passage of the relativistic plasma outflow through a cloud-like density enhancement could initiate such a flare.

In §2, we derive an equation for plasmoid dynamics in terms of the evolving comoving particle distribution functions. Reduction to well-known forms in the non-radiative and radiative regimes is performed in §3. Prescriptions for the energy transfer from nonthermal protons to electrons, which get us past the difficult particle acceleration and plasma physics which can be implemented in later studies, are proposed in §4. In §5, we treat the optically thin synchrotron radiation process, and effects of parameter changes are presented in §6. The results are examined analytically in §7, and application to GRBs and blazars is made in §8. We summarize in §9. A detailed numerical treatment is presented in a companion paper (Chiang & Dermer 1997b).

2. Plasmoid Dynamics

We consider the system shown in Fig. 1. A plasmoid, consisting of a volume of magnetized plasma, is located on the $\hat{x}$-axis at location x and moves with Lorentz factor $\Gamma(x)$. The comoving volume of the plasmoid is $V(x) \cong A(x)L(x)$, where $A(x)$ is the area of the plasmoid at x and $L(x)$ is the mean width of the plasmoid as measured in the comoving frame. The plasmoid travels through an external medium with density $n_{\rm ext}(x)$ which is assumed to be fully ionized electron-proton plasma. Consequently the plasmoid captures an electron-proton pair of the ISM gas if the proton Larmor radius is much smaller than the characteristic size scales (L and $A^{1/2}$) of the plasmoid. Except for chance collisions, neutral particles would pass through the plasmoid unless they are ionized by interactions with the plasmoid.

The plasmoid is assumed to consist initially of thermal lepton-proton plasma which was ejected from the GRB event. In our notation, $m_p = 1.5 \times 10^{-3}$ ergs and $m_e = 8.2 \times 10^{-7}$ ergs, so that the mass of the thermal particles in the plasmoid is just $\mathcal{M}_{\rm th} = m_p N_{\rm th}(1 + a_{\rm th})$, where $N_{\rm th}$ is the total number of protons in the plasmoid ejecta. The factor $a_{\rm th} = (1 + 2z_{\rm th})m_e/m_p$ corrects for the mass of electrons and pairs, the latter of which are assumed to be present in the ratio $z_{\rm th} = N_{\rm th,+}/N_{\rm th}$, where $N_{\rm th,+}$ is the number of thermal positrons. Here we assume that $k_{\rm B}T_e/m_e \ll 1$ and $k_{\rm B}T_p/m_p \ll 1$, so that the thermal kinetic energy is a small fraction of the rest mass energy of the particles.

We furthermore adopt the notation that $N_{p(e)}$ stands for the proton (electron) momentum distribution function $N_{p(e)}[p; x(t)]$ differential in dimensionless momentum $p \equiv \beta\gamma$ (not to be confused with the subscript p which stands for proton), and that $N'_{p(e)}$ stands for the spatial gradient $\partial N_{p(e)}[p; x(t)]/\partial x$ of the proton (electron) momentum distribution function, where t is the time in the comoving frame. If the nonthermal particles are isotropically distributed in the comoving frame (see discussion in Dermer & Schlickeiser 1993), then the relativistic mass $\mathcal{M}_{\rm nt}$ of nonthermal particles is given by

$$\mathcal{M}_{\rm nt} = m_p \int_0^\infty dp\, \gamma\, (N_p + a_{\rm nt}N_e)\,, \tag{1}$$

where $a_{\rm nt}(p; x) = [1 + 2z_{\rm nt}(p; x)]m_e/m_p$ is the additional relativistic mass in the form of nonthermal leptons, and $z_{\rm nt}(p)$ is the momentum-dependent pair ratio in the nonthermal lepton distribution.

The x-component of the relativistic momentum of the plasmoid at location x, denoted $\Pi_x(x)$, is given by $P(\mathcal{M}_{\rm th} + \mathcal{M}_{\rm nt})$, where $P = B\Gamma$ and Bc is the speed of the plasmoid. At $x + \delta x$, the total x-component of the momentum of the plasmoid, including the swept-up particles and radiated photons, is given by

$$\Pi_x(x + \delta x) = m_p(P + P'\delta x)\{(N_{\rm th} + N'_{\rm th}\delta x)(1 + a_{\rm th} + a'_{\rm th}\delta x)+$$
$$+ \int_0^\infty dp\, \gamma\, [N_p + N'_p\delta x + (a_{\rm nt} + a'_{\rm nt}\delta x)(N_e + N'_e\delta x)]\} - \frac{\delta x}{c}\int_0^\infty dp\, (\dot{\gamma}_p N_p + \dot{\gamma}_e N_e). \tag{2}$$

The last integral in this equation refers to the momentum carried by radiated photons, and is related to the internal particle distribution functions through the comoving frame energy-loss rates $m_p\dot{\gamma}_p$ and $m_e\dot{\gamma}_e$ of the protons and electrons, respectively. This formalism allows for particle creation and annihilation, although in this paper we assume for simplicity that $a'_{\rm th} = a'_{\rm nt} = 0$. We furthermore set $N'_{\rm th} = 0$ so that no particles are added to the thermal pool. This does not impose any loss of generality if the nonthermal particles are followed to nonrelativistic energies.

Expanding equation (2) in powers of δx, equating to $\Pi_x(x)$ by momentum conservation and retaining terms to first order in δx, we obtain the equation

$$-\frac{P'}{P} = \frac{\int_0^\infty dp\, \gamma(N'_p + a_{\rm nt}N'_e) - (cP)^{-1}\int_0^\infty dp\, (\dot{\gamma}_p N_p + \dot{\gamma}_e N_e)}{N_{\rm th}(1 + a_{\rm th}) + \int_0^\infty dp\, \gamma(N_p + a_{\rm nt}N_e)}\,. \tag{3}$$

The proton and electron injection function due to the plasmoid sweeping up particles from the ISM is given by

$$N'_{p,\mathrm{sw}} = n_{\mathrm{ext}} A \delta(p - P) = N'_{e,\mathrm{sw}} \; . \tag{4}$$

Equation (4) says that protons and electrons are injected into the comoving plasma with momenta $p = B\Gamma$ at a rate determined by the ISM density $n_{\mathrm{ext}}(x)$ and area $A(x)$ of the plasmoid. When radiation is important, the functions N'_p and N'_e in equations (2) and (3) contain terms in addition to the sweep-up functions (4) due to the evolution of the comoving particle distribution functions. By multiplying the particle continuity equation by γ and integrating over $d\gamma$, using the relation $dx = B\Gamma c\, dt$, we find that

$$\int_1^\infty d\gamma \; \gamma \{ \dot{N}(\gamma) + \frac{\partial[\dot{\gamma}N(\gamma)]}{\partial\gamma} \} = \int_1^\infty d\gamma \; [\gamma \dot{N}(\gamma) - \dot{\gamma}N(\gamma)] = B\Gamma c \int_1^\infty d\gamma \; \gamma N'_{\mathrm{sw}} \; , \tag{5}$$

noting that $[\gamma\dot{\gamma}N(\gamma)]|_1^\infty = 0$. Consequently the numerator in equation (3) contains only the contribution from the sweep-up function (4), and we arrive at the result

$$-\frac{P'}{P} = \frac{\int_0^\infty dp \; \gamma(N'_{p,\mathrm{sw}} + a_{\mathrm{nt}}N'_{e,\mathrm{sw}})}{N_{\mathrm{th}}(1 + a_{\mathrm{th}}) + \int_0^\infty dp \; \gamma(N_p + a_{\mathrm{nt}}N_e)} \; . \tag{6}$$

Note that we have neglected the energy content in magnetic field in equation (3) by assuming that it is small in comparison with that of the thermal and nonthermal particle energies. The importance of the magnetic energy term can be checked once the plasmoid volume is specified, and can be important if equipartition is assumed between the magnetic field and nonthermal particle energy densities. For the applications presented here, however, we assume that this term is negligible.

3. Asymptotic Behavior of $\Gamma(x)$

The relation between the comoving time t and spatial coordinate x is given by

$$\frac{1}{c} \int_{x_0}^x \frac{d\tilde{x}}{B(\tilde{x})\Gamma(\tilde{x})} = \int_{t_0}^t d\tilde{t} = t - t_0 \; . \tag{7}$$

The terms x_0 and t_0 in equation (7) stand for the initial location and comoving time when the parameter values are specified. The nonthermal power from swept-up protons and leptons is probably dominated by the proton component in the ISM environment surrounding a GRB source, though a substantial pair content could be found in the vicinity of supermassive black holes which power blazars. Assuming for simplicity that the swept-up matter is pair free, we can therefore write that the power injected in nothermal particles per unit comoving time is given by $\dot{E} = m_p \int_0^\infty dp \; \gamma \; \dot{N}_{p,\mathrm{sw}} = m_p B\Gamma c \int_0^\infty dp \; \gamma \; N'_{p,\mathrm{sw}}$. Using equation (4), we therefore see that the kinetic energy injected per unit time is

$$\dot{E}_{\mathrm{ke}} = m_p B(\Gamma^2 - \Gamma) c n_{\mathrm{ext}} A \tag{8}$$

(Blandford & McKee 1976), neglecting the power in swept-up electrons. Vietri (1997a,b) has used this equation to predict GRB afterglow behavior assuming that the bulk of the nonthermal particle energy is radiated on a time scale short compared to the time scale for the evolution of Γ, i.e., that the plasmoid is in the radiative regime.

When particle radiation is negligible, $\dot{\gamma}_p = \dot{\gamma}_e = 0$, and the evolution of the particle distribution function is entire due to the sweep-up nonthermal particles. Under these conditions, equation (6) reduces to

$$-\frac{P'}{P} \simeq \frac{n_{\mathrm{ext}}(x)A(x)\Gamma(x)}{N_{\mathrm{th}} + \int_0^x d\tilde{x} \; n_{\mathrm{ext}}(\tilde{x})A(\tilde{x})\Gamma(\tilde{x})} \; . \tag{9}$$

Equation (9) describes the dynamics of the plasmoid in the *non-radiative* regime [1]. If the particle kinetic energy is promptly radiated away, leaving behind only the rest mass of the initial and swept-up particles – which is dominated by the mass of the protons – then equation (6) reduces to

$$-\frac{P'}{P} \cong \frac{n_{\rm ext}(x)A(x)\Gamma(x)}{N_{\rm th} + \int_0^x d\tilde{x}\, n_{\rm ext}(\tilde{x})A(\tilde{x})} \ . \tag{10}$$

This equation describes the dynamics of the plasmoid in the *radiative* regime.

3.1. Non-Radiative Regime

Asymptotic forms for plasmoid dynamics in the non-radiative and radiative regime are simply derived for a relativistic ($\Gamma \gg 1$) plasmoid. We parameterize the plasmoid area by the expression

$$A = A_0(\frac{x}{x_0})^j = 4\pi x_0^2 f_b(\frac{x}{x_0})^j \ , \tag{11}$$

where $f_b = \delta\Omega/4\pi$ is a collimation (or beaming) factor and $\delta\Omega$ is the solid angle into which the plasmoid is directed. Equation (11) reduces to an uncollimated blast wave when $j = 2$ and $f_b = 1$. We parameterize the spatial dependence of the external density distribution by the expression

$$n_{\rm ext}(x_i) = n_0(\frac{x}{x_0})^{-\eta} \ , \tag{12}$$

and assume that the plasmoid Lorentz factor follows the power-law behavior

$$\Gamma(x) = \Gamma_0(\frac{x}{x_0})^{-g} \ , \tag{13}$$

where Γ_0 is the initial plasmoid Lorentz factor.

In the early free-expansion stage, the plasmoid is ballistic so that $\Gamma(x) = \Gamma_0$. Transition to power-law behavior in both the non-radiative and radiative regimes occurs when the relativistic mass $\mathcal{M}_{\rm sw}\Gamma_0$ of the swept-up particles equals the original mass $m_p N_{\rm th}$ in the burst ejecta. This occurs when

$$\int_0^{x_0} d\tilde{x}\, n_{\rm ext}(\tilde{x})A(\tilde{x})\Gamma(\tilde{x}) \cong \Gamma_0 \int_0^{x_0} d\tilde{x}\, n_{\rm ext}(\tilde{x})A(\tilde{x}) \geq N_{\rm th} = \frac{E_0}{\Gamma_0 m_p} \ , \tag{14}$$

where the equality on the right-hand-side relates the initial energy $E_0 = 10^{50}E_{50}$ ergs of the GRB explosion or blazar flare to $N_{\rm th}$. One finds that

$$x_0 = [\frac{(j + 1 - \eta)E_0}{4\pi f_b n_0 \Gamma_0^2 m_p}]^{1/3} = 3.9 \times 10^{15}[\frac{(j + 1 - \eta)E_{50}}{f_b n_0 \Gamma_{300}^2}]^{1/3} \ {\rm cm} \ , \tag{15}$$

where $\Gamma_{300} = \Gamma_0/300$. This reduces to the result of Rees & Mészáros (1992) when $j = 2$, $\eta = 0$, and $f_b = 1$.

Substituting equations (11)-(13) into equation (9), one obtains

$$-\frac{\Gamma'}{\Gamma} = \frac{g}{x} = \frac{j - g - \eta + 1}{x} \ , \tag{16}$$

---

[1] This limit is also commonly referred to as the adiabatic regime. We avoid use of this term which can be confused with the early phases of the fireball expansion where adiabatic losses dominate the energy evolution of particles in the comoving frame.

so that equation (9) has a power-law solution in the non-radiative regime provided

$$g \to g_a = \frac{j + 1 - \eta}{2} \ . \tag{17}$$

Note that the index g_a in the non-radiative regime equals $3/2$ for the blast-wave case with uniform external density ($\eta = 0$). The power-law behavior persists until the plasmoid reaches location x_f defined by $\Gamma(x_f) \approx 1$. For the asymptotic form (13), we have

$$x_f = \Gamma_0^{1/g} x_0 \ . \tag{18}$$

3.2. Radiative Regime

The plasmoid Lorentz factor in the fully radiative regime follows power-law behavior for $x_0 \lesssim x \lesssim x_f$, where x_f is the location at which the mass of the swept-up matter equals the initial rest mass of particles in the GRB ejecta. When $N_{\rm th} \gg \int_0^x d\tilde{x} \, n_{\rm ext}(\tilde{x}) A(\tilde{x})$, we can simply see from equation (10) that $-d\Gamma/\Gamma^2 \propto x^{j-\eta} dx$, so that

$$g \to g_r = j + 1 - \eta = 2g_a \ . \tag{19}$$

Alternately, we can solve equation (10) directly when the integral in the denominator on the right-hand-side of equation (8) can be neglected. For a blast-wave geometry in a uniform external medium, $g_r = 3$ (Blandford & McKee 1976; see also Rees & Mészáros 1992; Mészáros et al. 1997). The power-law behavior in the radiative regime ends at the location x_f determined by the condition

$$N_{\rm th} = \int_{x_0}^{x_f} d\tilde{x} \, n_{\rm ext}(\tilde{x}) A(\tilde{x}) \ . \tag{20}$$

If $x_f \gg x_0$, this implies

$$\frac{x_f}{x_0} = \left(\frac{E_0 g_r}{\Gamma_0 m_p n_0 A_0 x_0} \right)^{1/g_r} \ . \tag{21}$$

The power-law behavior ends when $\Gamma(x_f) \approx 1$. Using equations (18) and (19), we therefore find that x_0 is also given by equation (15) in the radiative regime. Figure 2 shows a numerical solution of $\Gamma(x)$ along with the asymptotic forms in the radiative and non-radiative regimes for our standard parameter values $\Gamma_{300} = 1$, $n_0 = 1 \ {\rm cm}^{-3}$, $E_{50} = 1$, $j = 2$, $\eta = 0$, and $f_b = 1$ (see Table 1).

4. Energy Transfer from Protons to Electrons

The bulk of the energy injected into a relativistic plasmoid which sweeps up matter from the ISM is carried by nonthermal protons, yet in all likelihood the dominant radiation process in GRB afterglows is nonthermal electron synchrotron radiation (see, e.g., Waxman 1997a; Tavani 1997; Katz & Piran 1997; and discussion in Chiang & Dermer 1997a). It is also generally thought that the bulk of the radio-through-optical blazar emission is nonthermal electron synchrotron radiation. A mechanism transfers the energy from the proton to the electron population, for example, through shocks or the excitation of plasma wave turbulence by the protons which gets channeled into the electrons through gyroresonant coupling. We avoid the complicated microphysical details of the energy transfer process by offering two simple prescriptions for the transfer of energy from the protons to the electrons.

In the first prescription, we assume that a fraction ξ_{pe} of the kinetic energy power of the swept-up nonthermal protons in the comoving frame is instantaneously transformed into a "shock"-like momentum power-law electron distribution with index s. Hence

$$\dot{E}_e = \xi_{pe}(x)\dot{E} = m_e K(x) \int_{p_{\min}}^{p_{\max}} dp\,(\gamma - 1)p^{-s} = m_e K(x)f. \tag{22}$$

Naive shock acceleration theory predicts $s \geq 2$ and $s = 2$ for strong shocks in nonrelativistic gases (e.g. Jones & Ellison 1991). Consideration of relativistic gases and inclusion of nonlinear effects can produce harder power law injection with $s > 1$ (e.g. Ellison, Jones, & Reynolds 1990), and stochastic gyroresonant acceleration can produce extremely hard power-law and even quasi-monoenergetic spectra (see Schlickeiser, Campeanu, & Lerche 1993). In equation (22), the normalization coefficient $K = \xi_{pe}\dot{E}/fm_e$, where

$$f = \int_{p_{\min}}^{1} dp\,(\gamma - 1)p^{-s} + \int_{1}^{p_{\max}} dp\,(\gamma - 1)p^{-s} \cong \frac{1 - p_{\min}^{3-s}}{2(3-s)} + \frac{p_{\max}^{2-s} - 1}{2-s}, \tag{23}$$

provided $p_{\min} \ll 1$ and $p_{\max} \gg 1$. If $p_{\min} \gg 1$, then

$$f \cong \frac{p_{\max}^{2-s} - p_{\min}^{2-s}}{2-s}. \tag{24}$$

A second prescription for the energy transfer from protons to electrons is

$$\dot{E}_e = \frac{E_{p,\mathrm{ke}}}{\tau_{pe}}, \tag{25}$$

where

$$E_{p,\mathrm{ke}} = m_p \int_{0}^{\infty} dp\,(\gamma - 1)N_p. \tag{26}$$

Note that the energy transfer time scale τ_{pe} and the total proton kinetic energy $E_{p,\mathrm{ke}}$ are x- (or equivalently t-) dependent quantities. The second prescription is probably a better representation of the actual physics of the situation but affords less analytic development. The limit of complete, prompt energy transfer from the protons to the electrons corresponds to $\xi_{pe} \to 1$ and $\tau_{pe} \to 0$ in the first and second prescriptions, respectively.

The electron injection function at time t_i in the comoving frame for the first prescription is therefore

$$\dot{N}_e(p_i, t_i) = K\,p_i^{-s}\Theta(p_i; p_{\min}, p_{\max}) = \frac{\xi_{pe}m_p cB(\Gamma^2 - \Gamma)n_{\mathrm{ext}}A}{m_e f}\,p_i^{-s}\Theta(p_i; p_{\min}, p_{\max}), \tag{27}$$

where p_i is the injection momentum and $\Theta(p; p_{\min}, p_{\max})$ is the Heaviside function defined by $\Theta(x; x_1, x_2) = 1$ for $x_1 \leq x < x_2$ and $\Theta(x; x_1, x_2) = 0$ otherwise.

The evolution of the electron energy through synchrotron radiation is governed by the well-known equation

$$-\dot{\gamma} = \frac{4}{3}c\sigma_{\mathrm{T}}u_{\mathrm{H}}p^2 = \nu p^2, \quad u_{\mathrm{H}} = \frac{H^2}{8\pi m_e c^2}, \tag{28}$$

assuming an isotropic electron pitch-angle distribution. We also suppose that the magnetic field is randomly oriented with mean field strength H in our spectral calculations. In general, $H = H(x)$. The evolution of H with x involves subtleties. The assignment of an equipartition strength in GRB studies depends on knowledge of the local density which can be obtained through the shock jump conditions (e.g., Waxman

1997a; Mészáros et al. 1997). The magnetic field could be generated through turbulent field growth, or evolve from the original field in the plasmoid (Mészáros et al. 1994), for example, by flux freezing (see Chiang & Dermer 1997a). Our major simplification in the present study is to examine the case $H = H_0$ and $\nu = \nu_0 = \sigma_T c H_0^2/(6\pi m_e c^2)$, with H_0 and ν_0 independent of x. We are also mostly interested in the radiation from relativistic electrons ($p \gg 1$), in which case the electron equation of motion $-\dot{p} = \nu_0 p^2$ has the solution

$$p = p(t) = [p_i^{-1} + \nu_0(t - t_0)]^{-1} \tag{29}$$

(see Dermer & Schlickeiser 1993 for a related treatment; Sturner, & Schlickeiser 1997 for a treatment of Coulomb, bremsstrahlung, and Compton losses in addition to synchrotron losses; and Gould 1975, Goldshmidt & Rephaeli 1994, Dermer & Skibo 1997, and Chiang & Dermer 1997a for a consideration of adiabatic energy losses of the nonthermal electrons). Here we treat only the effects of synchrotron losses on the evolution of the electron spectra.

The electron distribution at time t resulting from the superposition of nonthermal electron power-law injection functions described by equation (27) over the time interval $t_0 \leq t_i \leq t$ is therefore

$$N_e(p; t) = \int_{t_0}^{t} dt_i \, \dot{N}_e(p, t_i) = p^{-2} \int_{\max[t_0, t - \nu_0^{-1}(p^{-1} - p_{\max}^{-1})]}^{t} dt_i \, K \, [p^{-1} - \nu_0(t - t_i)]^{s-2} , \tag{30}$$

where we assume that $p_{\min}$ and $p_{\max}$ are independent of t. We note that a value for $p_{\max}$ can be obtained in shock acceleration theory by balancing radiative loss and energy gain rates (e.g., Reynolds 1996).

We now follow the evolution of the nonthermal electron distribution that occurs over the period when the plasmoid Lorentz factor is described by the power-law asymptote (13). Integrating equation (7) from the onset of the power-law behavior at x_0 to location x_i, we find that

$$\frac{x_i}{x_0} = [\omega(t_i - t_0) + 1]^{1/(1+g)} , \tag{31}$$

where $\omega = (g + 1)\Gamma_0 c/x_0$. In the range $x_0 \leq x_i \leq x_f$, Γ, A, and n_{ext} are described by equations (13), (11), and (12), respectively. Thus

$$K \cong \frac{\xi_{pe} m_p c \Gamma_0^2 n_0 A_0}{m_e f} \left(\frac{x_i}{x_0}\right)^{j-2g-\eta} , \tag{30}$$

when $\Gamma \gg 1$.

In this regime, equation (27) becomes

$$N_e(p; \tau) = \frac{\xi_{pe} m_p c \Gamma_0^2 n_0 A_0}{m_e f p^2} \, I_s(\tau) \tag{33}$$

where

$$I_s(\tau) = \int_0^{\min[\tau, \nu_0^{-1}(p^{-1} - p_{\max}^{-1})]} dy \, (1 + \omega\tau - \omega y)^u \, (p^{-1} - \nu_0 y)^{s-2} . \tag{34}$$

Here $\tau = t - t_0$ and $u = (j - 2g - \eta)/(1 + g)$ (the integration variable $y = t - t_i$). The simplest case is given by $s = 2$, which corresponds to the strong shock index in the quasilinear regime of shock acceleration theory. When $s = 2$, equation (34) becomes

$$I_2(\tau) = \begin{cases} [\omega(1 + u)]^{-1}[(1 + \omega\tau)^{c_0} - (1 + \omega\tau - \omega\bar{y})^{c_0}], & \text{if } c_0 \neq 0; \\ \omega^{-1} \ln\left(\frac{1 + \omega\tau}{1 + \omega\tau - \omega\bar{y}}\right), & \text{if } c_0 = 0, \end{cases} \tag{35}$$

where $\bar{y} = \min[\tau, \nu_0^{-1}(p^{-1} - p_{\max}^{-1})]$ and $c_0 = 1 + u = (g_r - g)/(g + 1)$, recalling definition (19).

5. Synchrotron Radiation

The synchrotron emissivity in the comoving frame is treated in the δ-function approximation of Dermer & Schlickeiser (1993; eq.[5.16]), which we write as

$$\dot{N}_{\text{syn,com}}(\epsilon, \tau) = \frac{\nu_0}{\epsilon} \int_0^\infty dp\, p^2\, N_e(p; \tau) \delta[p - (\frac{\epsilon}{\epsilon_{\text{H}}})^{1/2}] = \frac{\nu_0}{2\epsilon_{\text{H}}^2} (\frac{\epsilon_{\text{H}}}{\epsilon})^{1/2}\, N_e[(\frac{\epsilon}{\epsilon_{\text{H}}})^{1/2}; \tau]\,. \tag{36}$$

The dimensionless cyclotron energy $\epsilon_{\text{H}} = H/H_{\text{cr}}$, where $H_{\text{cr}} = 4.414 \times 10^{13}$ Gauss. For a power-law electron distribution, approximation (36) is accurate everywhere except near the endpoints of the synchrotron spectrum. Self-absorption of the synchrotron radiation and synchrotron self-Compton emission (see Dermer, Sturner, & Schlickeiser 1997 for a treatment of the latter process) are not considered here.

The relationship between the observer's time element δt_{obs} and the comoving time element δt is $\delta t_{\text{obs}} = \delta t(1 + z)/\mathcal{D}$, where the Doppler factor $\mathcal{D} = [\Gamma(1 - B\mu_{\text{obs}})]^{-1}$ and $\arccos \mu_{\text{obs}}$ is the angle between the direction of travel of an emission element and the observer's line-of-sight. We consider the case where a portion of the plasmoid is directed along the line-of-sight to the observer, so that the received radiation is produced primarily by emitting plasma which is directed within a line-of-sight angle $\arccos \mu_{\text{obs}} \lesssim 1/\Gamma$ (see Chiang & Dermer 1997a when this is not the case). Thus we can let $\delta t_{\text{obs}} \to \delta t(1 + z)/\Gamma$. [2]

The observed photon energy (in units of m_e) is given by $\epsilon_{\text{obs}} = \mathcal{D}\epsilon/(1 + z) \to \Gamma\epsilon/(1 + z)$, where the last relation again holds for the emitting plasmoid directed within an angle $\arccos \mu_{\text{obs}} \lesssim 1/\Gamma$ of the observer's line-of-sight. The number of photons produced per unit observer's time per unit observed photon energy ϵ_{obs} is therefore given by

$$\dot{N}_{\text{syn}}(\epsilon_{\text{obs}}, t_{\text{obs}}) = \dot{N}_{\text{syn,com}}[\epsilon(\epsilon_{\text{obs}}), t(t_{\text{obs}})]\,, \tag{37}$$

noting that the Jacobian is unity. The quantity $\dot{N}_{\text{com}}(\epsilon, t)$ is the differential photon production rate in the comoving frame.

In equation (37), we replace ϵ by $(1 + z)\epsilon_{\text{obs}}/\Gamma$ and t by a function of t_{obs} defined through the expression

$$t_{\text{obs}} - t_{\text{obs},0} = \tau_{\text{obs}} = (1 + z) \int_{t_0}^t \frac{d\tilde{t}}{\Gamma(\tilde{t})}\,. \tag{38}$$

In the power-law regime for the plasmoid Lorentz factor, equations (38), (13) and (31) imply

$$\omega\tau = (\Omega\tau_{\text{obs}} + 1)^{c_1} - 1\,, \tag{39}$$

where $\Omega = \omega\Gamma_0(1 + 2g)/[(1 + z)(1 + g)] = (2g + 1)c\Gamma_0^2/[x_0(1 + z)]$ and $c_1 = (1 + g)/(1 + 2g)$.

6. Numerical Results

We may now calculate the observed synchrotron radiation spectrum using equations (33) and (36) in equation (37). The power-law solution for Γ becomes accurate after observer's time

$$t_{\text{obs}} \gtrsim \Omega^{-1} \cong 1.4\, \frac{1 + z}{\Gamma_{300}^{8/3}(2g + 1)}\, (\frac{g_r E_{50}}{f_b n_0})^{1/3}\ \text{sec} \tag{40}$$

---

[2] At a fixed observer's time, the mean value of μ for a shell which emits uniformly per unit surface and expands with constant Lorentz factor is equal to B and $4B/(3 + B^2)$ for photons emitted isotropically in the comoving frame with energy index α equal to 0 and 1, respectively. When $\mu_{\text{obs}} \approx B$, $\mathcal{D} \cong \Gamma$.

following the start of the GRB, which represents only a couple seconds for our standard parameters (see eq.[15] and Table 1). A value of $p_{\max} = 10^7/H_0^{1/2}$ is used, which is consistent with a maximum synchrotron photon energy $\lesssim 25$ MeV in the comoving frame of expected from diffusive shock acceleration (de Jager & Baring 1997). The solution is no longer valid when $\Gamma \approx 1$, and we stop our calculations there.

Figure 3 illustrates the relationship between Γ/Γ_0 and x/x_0 as a function of the quantity $\Omega t_{\rm obs}$. As expected, a highly radiative blast wave in a uniform external medium (i.e., $g = 3$) slows down most rapidly and travels the shortest distance. When $g < 3$, due either to a non-blast wave geometry with $j < 2$, a thinning external medium with $\eta > 0$, or inefficient radiation of the swept-up nonthermal proton energy, the plasmoid decelerates more slowly.

The spectra at different observing times and the time profiles at different observed photon energies are presented in Figures 4-6. The spectra are plotted at observing times $t_{\rm obs} = 1$, 10, 10^2 sec, etc., from top to bottom. The spectra show a spectral hardening from photon energy index $\alpha = 1/2$ at lower photon energies to $\alpha \gtrsim 1$ at higher photon energies due to the effects of cooling on the spectra for the index $s = 2$ used in the electron momentum spectrum. Spectra measured at late times display a spectral break at lower photon energies because the effects of cooling on the lower energy electrons are only felt at late times. A pile-up appears at the spectral break, and this pile-up becomes more pronounced at later times and lower photon energies as more electrons are swept into the pile-up region.

Figure 4 shows the spectra and time profiles using all standard parameters (see Table 1). The standard value of 10 Gauss for the magnetic field is arbitrarily assigned in order to provide a spectral break at ≈ 100 keV - several MeV, as is typical for many GRBs (e.g., Band et al. 1993). The parameters in Figure 5 are the same as those in Figure 4 except that $H_0 = 1$ Gauss. This has the effect of moving the energy of the spectral break to higher energies at comparable observing times. Figure 6 shows a calculation using all standard parameters except for $\Gamma_0 = 30$, $n_0 = 0.01$ cm^{-3}, and a beaming factor $f_b = 0.01$. This choice delays the onset of the asymptotic power-law regime to late times (compare eq.[40]), and is driven by an attempt to explain observations of the peaking of the optical and X-ray afterglow emission of GRB 970508 at ≈ 2 days following the burst.

The time profiles of Figures 4-6 can be understood qualitatively as follows: The highest photon energies are produced by very energetic electrons. In the comoving frame, only the most recently injected high-energy electrons have not been degraded to lower energies by synchrotron cooling. The time profile of the decay at MeV - GeV energies is therefore determined by the power in recently injected electrons, which reflects the time-dependence of the power in the swept-up matter as the plasmoid decelerates. The time profiles in this regime follow a power law behavior $\propto t_{\rm obs}^{-\chi}$, with slope $\chi \approx 10/7$, as explained in the next section. The electrons which produce synchrotron radiation at lower observed photon energies take much longer to cool. Before cooling is important, these electrons accumulate. The time profiles in this regime consequently decay more slowly than in the strongly cooled regime. The slope of the time profile reflects both the accumulation of newly injected electrons and Doppler effects on the observer. Because the plasmoid is decelerating, synchrotron emission at a fixed observing energy is produced increasingly by the fewer higher energy electrons.

The spectra in Figs. 4-6 are presented in the dimensionless form $\nu L_\nu/m_e$, and reach values of $10^{52} - 10^{54}$ during the first 1-100 seconds of the GRB. The weakest GRBs observed with BATSE are triggered at thresholds of ≈ 0.2-1 photon cm^{-2} s^{-1} in the 50-300 keV range. For a mean photon energy of 100 keV for GRB sources at a distance of 10^{28} cm, roughly corresponding to $z = 1$, we would therefore expect $\nu L_\nu/m_e$ fluxes of $\approx (0.2 - 1) \times 4\pi \times 10^{56} \times 0.1/0.511 \cong 5 \times 10^{55} - 3 \times 10^{56}$. Consequently, the

energetics can be explained only if a typical GRB involves at least 10^{52} ergs or if $f_b \lesssim 0.01$ and $\Omega^{-1} \sim$ 1-10 sec.

There is a characteristic time $\hat{\tau}_{\rm obs}$ when synchrotron cooling starts to influence the total number of electrons which produce radiation at a given energy. The value of $\hat{\tau}_{\rm obs}$ is longer at lower photon energies, and this effect causes the X-ray to γ-ray flux ratio to rapidly increase during the first 100 seconds in Figures 4 and 5. For this model with constant magnetic field, the light curve of the decaying gamma-ray emission asymptotically approaches a power-law with slope characteristic of the cooled regime.

7. Analytic Interpretation

Equation (39) can be rewritten in terms of a dimensionless time $\mathtt{T} = 1 + \Omega\tau_{\rm obs}$ through the expression

$$1 + \omega\tau = \mathtt{T}^{c_1} . \tag{41}$$

From equations (13) and (31),

$$\Gamma = \Gamma_0 \mathtt{T}^{-c_2} , \tag{42}$$

where $c_2 = g/(2g+1)$. We also write

$$p^2 = \frac{\epsilon}{\epsilon_{\rm H}} = \left[\frac{(1+z)\epsilon_{\rm obs}}{\Gamma_0 \epsilon_{\rm H}}\right] \mathtt{T}^{c_2} = \mathcal{E}\mathtt{T}^{c_2} . \tag{43}$$

Equation (37) becomes, with equation (33) and (36),

$$\dot{N}_{\rm syn}(\mathcal{E}, \mathtt{T}) = \frac{\nu_0 K_0}{2\epsilon_{\rm H}^2 \Omega} \mathcal{E}^{-3/2} \mathtt{T}^{-3c_2/2} I_s(\mathtt{T}) , \tag{44}$$

where

$$K_0 = \frac{\xi_{\rm pe} m_p \epsilon_{\rm H} c \Gamma_0^3 n_0 A_0}{(1+z)m_e f} . \tag{45}$$

In the uncooled regime, $\tau \ll \nu_0^{-1}(p^{-1} - p_{\max}^{-1})$. Examination of equation (34) shows that when $p \ll p_{\max}$,

$$I_s(\mathtt{T}) \to I_s^{\rm uncooled} = \frac{p^{2-s}}{c_0 \omega}(\mathtt{T}^{c_0 \cdot c_1} - 1) . \tag{46}$$

Equation (45) applies for all values of $c_0 \neq 0$; when $c_0 = 0$, $I_s^{\rm uncooled} = \omega^{-1} c_1 \ln \mathtt{T}$. The time-dependence of the energy spectrum of the synchrotron radiation in the regime where the emission is produced mainly by electrons which have not cooled through synchrotron radiation is given by

$$\dot{N}_{\rm syn}^{\rm uncooled}(\mathcal{E}, \mathtt{T}) = \frac{\nu_0 K_0}{2c_0 \epsilon_{\rm H}^2 \Omega \omega} \mathcal{E}^{-(s+1)/2} \mathtt{T}^{-c_2(s+1)/2} (\mathtt{T}^{c_0 \cdot c_1} - 1) . \tag{47}$$

The regime where the bulk of the injected electrons has already cooled is characterized by the condition $\tau \gg \nu_0^{-1}(p^{-1} - p_{\max}^{-1})$. When $p \ll p_{\max}$,

$$I_s(\mathtt{T}) \to I_s^{\rm cooled} = \frac{p^{1-s}}{(s-1)\nu_0} \mathtt{T}^{c_1 \cdot (c_0 - 1)} , \tag{48}$$

and the observed synchrotron flux is given by

$$\dot{N}_{\rm syn}^{\rm cooled}(\mathcal{E}, \mathtt{T}) = \frac{K_0}{2(s-1)\epsilon_{\rm H}^2 \Omega} \mathcal{E}^{-(s+2)/2} \mathtt{T}^{-c_2(s+2)/2 + c_1 \cdot (c_0 - 1)} . \tag{49}$$

From the above results, we see that the negative of the slopes of the synchrotron flux time profiles produced by a decelerating plasmoid in the asymptotic power law regimes $t_{\rm obs} \gg \Omega^{-1}$ are given by

$$\chi_{\rm uncooled} = -c_0 \cdot c_1 + c_2(s+1)/2 \to c_2(s+1)/2 \,, \tag{50}$$

and

$$\chi_{\rm cooled} = -c_0 \cdot c_1 + c_1 + c_2(s+2)/2 \to c_1 + c_2(s+2)/2 \,, \tag{51}$$

in the uncooled and cooled regimes, respectively. The expressions on the right-hand-side of equations (50) and (51) represent the fully radiative regime where $g = g_r$ and, therefore, $c_0 = 0$. Table 2 shows the derived slopes of the flux time profiles for emission in the fully radiative uncooled and cooled regimes When $g < g_r$, which happens when the incoming energy is not fully radiated – and which must be the case in view of the fact that there are still some nonthermal electrons which are radiating energy – the slopes are less negative than given here, so that the profiles decay more slowly. A numerical calculation (Chiang & Dermer 1997b) is required to determine the slopes of the time profiles in this regime. In the extreme non-radiative regime, where $g = g_a = g_r/2$, the amount of radiated energy is negligible, and the slopes of the time profiles are harder by $c_0 \cdot c_1 = g/(2g+1)$ units. The derived slopes in the fully non-radiative regime are also listed in Table 2, as well as the difference in slopes between the cooled and uncooled regimes. These differences are the same in the radiative and non-radiative limits.

The transition from the regime where synchrotron cooling plays a negligible role to the regime where it plays a major role in determining the number of nonthermal electrons with momentum p occurs at comoving time $\hat{\tau} \approx (\nu_0 p)^{-1}$, provided $p \ll p_{\rm max}$. This also yields the observer time $\hat{\tau}_{\rm obs}$ when synchrotron cooling starts to strongly regulate the number of electrons which produce synchrotron emission at some observed energy. For times $\hat{\tau} \gg \omega^{-1}$ or, equivalently, $\hat{\tau}_{\rm obs} \gg \Omega^{-1}$, we can use equation (41) to write $\hat{\tau} = \omega^{-1}(\Omega\hat{\tau}_{\rm obs})^{c_1}$ and equation (43) to write p in terms of the observed photon energy $\epsilon_{\rm obs}$. After a tedious derivation, one obtains the result

$$\hat{\tau}_{\rm obs} = \frac{(1+z)^{1-c_3}(g+1)^{2c_3}433^{1-2c_3}(4.1 \times 10^6)^{c_3}}{300(2g+1)H_0^{3c_3}\epsilon_{\rm obs}^{c_3}} \, \Gamma_{300}^{(13c_3-8)/8} \, \Big(\frac{g_r E_{50}}{f_b n_0}\Big)^{(1-2c_3)/3} \,. \tag{52}$$

The term $g_3 = 1/(2c_1 + c_2) = (2g+1)/(3g+2)$. When $g = 3$,

$$\hat{\tau}_{\rm obs} \cong 8.5 \, \frac{(1+z)^{0.364}\Gamma_{300}^{0.034}}{H_0^{1.91}\epsilon_{\rm obs}^{0.636}} \, \Big(\frac{f_b n_0}{E_{50} g_r}\Big)^{0.0909} \; {\rm sec} \,. \tag{53}$$

When $g = 1$,

$$\hat{\tau}_{\rm obs} \cong 7.0 \, \frac{(1+z)^{0.4}}{H_0^{1.8}\epsilon_{\rm obs}^{0.6}\Gamma_{300}^{0.025}} \, \Big(\frac{f_b n_0}{E_{50} g_r}\Big)^{0.0667} \; {\rm sec} \,. \tag{54}$$

The time at which synchrotron cooling effects begin to play an important role are very weakly dependent upon all parameters except H_0 and the observed photon energy $\epsilon_{\rm obs}$. The accuracy of equation (53) can be checked against Figs. 4 and 5 using $g_r = g = 3$. In Fig. 6, the Mészáros-Rees timescale Ω^{-1} is longer than $\hat{\tau}_{\rm obs}$, so that synchrotron cooling effects are always important by the time the plasmoid Lorentz factor enters the power-law asymptote regime described by equation (13).

8.   Discussion

8.1. Application to Gamma Ray Bursts

We use our results to make preliminary comparison with observations of delayed afterglow behaviors of GRBs noting, however, that a detailed numerical scheme is required to calculate accurately the time profiles of the afterglows. It seems likely that the X-ray and optical GRB afterglow emission is primarily observed in the regime where synchrotron cooling plays an important role in the nonthermal electron content which produces this radiation (see eqs.[53] and [54]). From Table 2, we see that the slopes of the time profiles in this "cooled" regime, whether in the non-radiative limit or the radiative limit, are fairly narrowly bracketed. Irrespective of the electron injection index s in the range $1 < s < 3$, the slopes χ lie between the values of $11/14 = 0.78$ and $23/14 = 1.64$. If the optical and X-ray afterglow indeed occur in the regime where synchrotron cooling is important, then $s = 2\alpha$ (see eq.[49]). For GRB 970228, $\alpha \cong 0.63$ (e.g. Waxman 1997a), and for GRB 970508, $\alpha \cong 0.65$ (Djorgovski et al. 1997), implying $s \cong 1.3$ in both cases. Such a spectrum can be produced by nonlinear effects in a relativistic shock (Ellison et al. 1990). The radiative regime with $g = g_r$ is suggested on energetic grounds (Vietri 1997b). From Table 2, we see that a relativistic blast wave decelerating in a uniform medium yields temporal slopes in the range $17/14 = 1.21 \lesssim \chi \lesssim 37/28 = 1.32$ when $1 < s < 1.5$. These values are in striking accordance with the slopes of the measured afterglow behaviors (see §1), particularly in view of an additional hardening of the temporal slopes expected from the fact that the radiative regime can never fully be achieved.

Against the apparent successes of the relativistic blast wave model in explaining the slopes of the afterglow time profiles, several difficulties must be mentioned: (1) The characteristic GRB spectral shape cannot be reproduced with the model presented here, which gives a $1/2$ power break due to incomplete synchrotron cooling rather than a more typical break of about one unit from the hard X-rays to the soft gamma rays. This problem can be ameliorated by the inclusion of relativistic shock effects which produce time-varying equipartition magnetic fields and shock-heated low-energy cutoffs in the electron momentum distribution, and will be dealt with elsewhere (Chiang & Dermer 1997b). (2) The short time-scale variability and the large diversity of GRB time profiles are not accounted for here, and probably cannot result from variations in the external medium (Fenimore, Madras, & Nayakshin 1996; Sari & Piran 1995), though internal shocks may suffice (see Kobayashi, Piran, & Sari 1997). (3) The tendency of the peak in the νF_ν spectrum of GRBs to be in the range 0.1-1 MeV – which is probably not due to selection effects (Harris & Share 1998) – remains unexplained by this model. (4) Finally, the peaking of the X-ray and optical time profiles two days after GRB 970508 is unexpected. Fig. 6 shows extreme parameters which produce a delayed peaking of the X-ray and optical ranges, but implies an accompanying long term gamma-ray production phase. The X-ray and optical feature at 2 days after GRB 970508 must therefore originate from another effect, for example by relativistic beaming due to a collimated plasmoid (Chiang & Dermer 1997a) or by a density enhancement which the expanding shell traverses as it decelerates.

8.2. Application to Blazars

The most extreme flaring behavior of blazars occurs in the gamma-ray regime, with luminosities L_f exceeding $10^{48} L_{48} f_b$ ergs s^{-1} and gamma-ray variability taking place on time scales $t_f \lesssim t_{\rm day}$ days, with $L_{48} \sim 1$ and $t_{\rm day} \lesssim 1$. The Eddington limit for a $10^8 M_8 M_\odot$ black hole is $\approx 10^{46} M_8$ ergs s^{-1}. If the jet luminosity represents a significant fraction of the Eddington luminosity and is collimated into 0.1 - 1% of the full sky, then $10^8 M_\odot$ black holes could power such flares. This interpretation is also consistent with a minimum variability time scale defined by the Schwarzschild radius of the black hole, which is about 15

minutes when $M_8 \sim 1$.

Interactions of the jet plasma with clouds in the external medium could provide a mechanism for transforming the kinetic energy of the jet power into the emitted radiation. Certain conditions have to be met for this interpretation to be valid. In particular, the clouds have to be (i) small enough to be in accord with the observed variability time scale, (ii) dense and massive enough to afford efficient conversion of the plasmoid energy into radiation, (iii) close enough to the central black hole so that a cloud can pass through the volume traversed by the jet on a time scale of order days, (iv) large enough to occult a large portion of the jet, and (v) numerous enough to agree with the blazar flare duty cycle.

Neglecting redshift factors in these estimates, we see that condition (i) implies that $r_{\rm cloud}/c\Gamma^2 \lesssim t_f$, so that the cloud radius $r_{\rm cloud} \lesssim 3 \times 10^{17}\Gamma_{10}^2 t_{\rm day}$ cm, where $\Gamma_{10} = \Gamma/10$. Assuming that the plasmoid is highly radiative, equation (8) gives $4\pi f_b d_{\rm cloud}^2 m_p \Gamma^2 c n_{\rm cloud} \gtrsim 10^{48} L_{48} f_b$, where $d_{\rm cloud} = 10^{16} d_{16}$ cm is the distance of the cloud from the supermassive black hole. Condition (ii) therefore implies that $n_{\rm cloud} \gtrsim 2 \times 10^5 L_{48}(\Gamma_{10} d_{16})^{-2}$ cm^{-3}. In the fully radiative limit, we see from equation (20) that a plasmoid will be decelerated to nonrelativistic speeds if the number of swept-up particles roughly equals the number of jet particles. Consequently we find that the cloud mass $M_{\rm cloud} \cong M_{\rm plasmoid} \cong L_f t_f/\Gamma$, so that $M_{\rm cloud} \gtrsim 10^{52} L_{48} f_b t_{\rm day}/\Gamma_{10}$ ergs. For a spherical cloud, we therefore see that $n_{\rm cloud} \gtrsim 10^9 L_{48} f_b t_{\rm day}/R_{15}^3 \Gamma_{10}$ cm^{-3}, where we define $R_{15} = r_{\rm cloud}/(10^{15}{\rm cm})$.

For condition (iii), we find that the cloud takes $\approx 1.7 d_{16}^{3/2}/M_8^{1/2}$ days to travel one degree if the clouds follow circular orbits, and could therefore traverse the jet opening angle on a time scale of several days for the given parameters. Condition (iv) is satisfied if $R_{15} \gtrsim d_{16}(\theta_j/0.1 {\rm rad})$, where θ_j is the jet opening angle. The duty cycle of flares is not well known due to the sparse sampling of blazars, but might be in the range of 1-10%. Condition (v) therefore translates into a covering factor of comparable value as the duty cycle.

The interpretation that blazar flares could result from relativistic plasma outflows interacting with clouds is therefore consistent with observations if marginally Thomson thick clouds of radii $\sim 10^{15}$ cm are located some hundreds to thousands of Schwarzschild radii from the central supermassive black holes.

9. Summary

A method is presented in this paper to treat the dynamics of a volume of relativistically moving magnetized plasma – a plasmoid – that sweeps up material from the interstellar medium and whose entrained nonthermal particles radiate their internal kinetic energy, thereby changing the relativistic inertia of the plasmoid. The formalism is cast in terms of particle distribution functions in the comoving plasmoid frame: these functions evolve when particles are swept-up, when energy is transferred between the hadronic and leptonic components in the plasmoid, and when energy is lost to radiation. Such an approach is open-ended in the sense that more complicated scenarios not dealt with here can be treated, such as the inclusion of other radiation processes (e.g., Compton scattering and bremsstrahlung, and secondary and photo-meson production), of diffusive escape of nonthermal particles from the plasmoid, and of pair and compactness effects and the microphysical details of particle acceleration within the plasmoid.

We have studied a highly idealized system consisting of a relativistic blast wave or plasmoid with a constant entrained magnetic field. Only optically-thin synchrotron processes were treated here, and it was assumed that a fixed fraction of the swept-up nonthermal proton energy is instantaneously transformed into a power-law nonthermal electron momentum spectrum. This model was completely solved in the limit

of a relativistic plasmoid whose Lorentz factor follows the power-law behavior given by equation (13). This solution can be used to benchmark numerical codes that include additional processes. Application of these results to studies of gamma-ray bursts and blazars was indicated, and will be developed more thoroughly in a numerical examination of the system.

Table 1: List of Parameters, their Standard Values, and Values of Derived Quantities

Parameter or Derived Quantity	Standard Value
$\Gamma = \Gamma_0(x/x_0)^{-g}$	$g = 3$
$\Gamma_0 = 300\Gamma_{300}$	$\Gamma_{300} = 1$
$n_{\text{ext}} = n_0(x/x_0)^{-\eta}$	$\eta = 0$
n_0	1 cm^{-3}
$E_{50} = E_0/10^{50} \text{ ergs}$	$E_{50} = 1$
$A = A_0(x/x_0)^j$	$j = 2$
f_b	1
H_0	10 Gauss
s	2
z	1
$g_r = j + 1 - \eta$	3
$g_a = (j + 1 - \eta)/2$	3/2
x_0	0.0018 pc
$A_0 = 4\pi x_0^2 f_b$	$3.9 \times 10^{32} \text{ cm}^{-2}$
ω^{-1}	156 sec
Ω^{-1}	0.58 sec

Table 2: Negative of Slopes of Time Profiles in Fully Radiative Regime $g = g_r = j + 1 - \eta$ and Fully Non-Radiative Regime $g = g_a = g_r/2$

	s = 1			s = 1.5			s = 2			s = 3		
g	1	2	3	1	2	3	1	2	3	1	2	3
c_1	2/3	3/5	4/7	2/3	3/5	4/7	2/3	3/5	4/7	2/3	3/5	4/7
c_2	1/3	2/5	3/7	1/3	2/5	3/7	1/3	2/5	3/7	1/3	2/5	3/7
$c_{\text{uncooled}}^{\text{rad}}$	1/3	2/5	3/7	5/12	1/2	15/28	1/2	3/5	9/14	2/3	4/5	6/7
$c_{\text{cooled}}^{\text{rad}}$	7/6	6/5	17/14	5/4	13/10	37/28	4/3	7/5	10/7	3/2	8/5	23/14
$c_{\text{uncooled}}^{\text{adi}}$	0	0	0	1/12	1/10	3/28	1/6	1/5	3/14	1/3	2/5	3/7
$c_{\text{cooled}}^{\text{adi}}$	5/6	4/5	11/14	11/12	9/10	25/28	1	1	1	7/6	6/5	17/14
Δc	5/6	4/5	11/14	5/6	4/5	11/14	5/6	4/5	11/14	5/6	4/5	11/14

REFERENCES

Band, D. L., et al. 1993, ApJ, 413, 281

Blandford, R. D., & McKee, C. F. 1976, Phys. Fluids, 19, 1130

Catanese, M. et al. 1997, ApJ Letters, in press

Chiang, J., & Dermer, C. D. 1997a, ApJ Letters, submitted (astro-ph/9708035)

Chiang, J., & Dermer, C. D. 1997b, in preparation

Costa, E., et al. 1997, Nature, 387, 783

de Jager, O. C., & Baring, M. G. 1997, in The Fourth Compton Symposium, ed. C. D. Dermer, M. S. Strickman, & J. D. Kurfess (New York: AIP), 171

Dermer, C. D., & Schlickeiser, R. 1993, ApJ, 416, 484

Dermer, C. D., Sturner, S. J., & Schlickeiser, R. 1997, ApJS, 109, 103

Dermer, C. D., & Skibo, J. G., 1997, in The Fourth Compton Symposium, ed. C. D. Dermer, M. S. Strickman, & J. D. Kurfess (New York: AIP), 1044

Djorgovski, S. G., et al. 1997, Nature, 387, 876

Ellison, D. C., Jones, F. C., & Reynolds, S. P. 1990, ApJ, 360, 702

Fenimore, E. E., Madras, C., & Nayakshin, S. 1996, ApJ, 473, 998

Fishman, G. J., & Meegan, C. A. 1995, ARAA, 33, 415

Frail, D. A., et al. 1997, Nature, 389, 261

Garcia, M. R., et al. 1997, ApJ Letters, submitted (astro-ph/9710346)

Galama, T., et al. 1997, Nature, 387, 479

Goldshmidt, O. & Rephaeli, Y. 1994, ApJ, 431, 586

Goodman, J. 1997, New Astronomy,2(5):449

Gould, R. J. 1975, ApJ, 196, 689

Harris, M. J., & Share, G. J. 1998, ApJ, in press

Hartman, R. C., Collmar, W., von Montigny, C., & Dermer, C. D., in The Fourth Compton Symposium, ed. C. D. Dermer, M. S. Strickman, & J. D. Kurfess (New York: AIP), 307

Jones, F. C., & Ellison, D. C. 1991, Space Sci. Rev., 58, 259

Katz, J. I., & Piran, T. 1997, ApJ, submitted (astro-ph/9706141)

Kobayashi, S., Piran, T., & Sari, R. 1997, ApJ, 490, 92

Mészáros, P., & Rees, M. J. 1993, ApJ, 405, 278

Mészáros, P., & Rees, M. J. 1997, ApJ, 476, 232

Mészáros, P., Rees M. J., & Papathanassiou, H. 1994, ApJ, 432, 181

Mészáros, P., Rees, M. J., & Wijers, R. A. M. J., 1997, ApJ, submitted (astro-ph/9709273)

Meegan, C. A., et al. 1992, Nature, 355, 143

Metzger, M. R., et al. 1997, Nature, 387, 878

Michelson, P. F., et al. 1994, in The Second Compton Symposium, ed. C. E. Fichtel, N. Gehrles, & J. P. Norris (New York: AIP), 602

Panaitescu, A., & Mészáros, P. 1997, ApJ, in press (astro-ph/9703187)

Piro, L., et al. 1997, A&A, submitted (astro-ph/9710355)

Rees, M. J., & Mészáros, P., 1992, MNRAS, 258, 41P

Reynolds, S. P. 1996, ApJ, 459, L13

Schlickeiser, R., Campeanu, A., & Lerche, I. 1993, A&A, 276, 614

Sahu, K. C., et al. 1997, ApJ, 489, L127

Sari, R., & Prian, T. 1995, ApJ, 455, L143

Shrader, C. R., & Wehrle, A. E., in The Fourth Compton Symposium, ed. C. D. Dermer, M. S. Strickman, & J. D. Kurfess (New York: AIP), 328

Tavani, M. 1997, ApJ, 483, L87

van Paradijs, J., et al. 1997, Nature, 386, 686

Vietri, M. 1997a, ApJ, 478, L9

Vietri, M. 1997b, ApJ, 488, L105

Waxman, E. 1997a, ApJ, 485, L5

Waxman, E. 1997b, ApJ, 489, L33

Wijers, R. A. M. J., Rees, M. J., & Mészáros, P., 1997, MNRAS, 288, L51
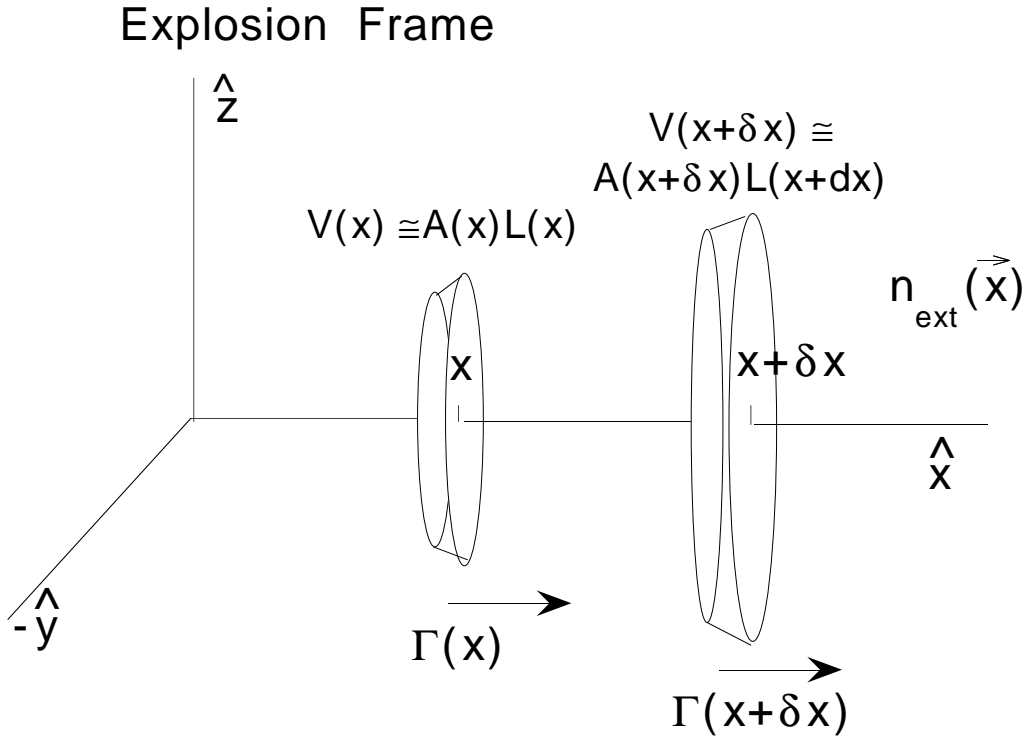
Fig. 1.— Cartoon illustrating the geometry of the plasmoid outflow and deceleration. The variation of the plasmoid bulk Lorentz factor $\Gamma(x)$ with location x depends on the amount of swept-up external matter, which is characterized by density $n_{\mathrm{ext}}(\mathbf{x})$, and the amount of internal energy which is radiated.
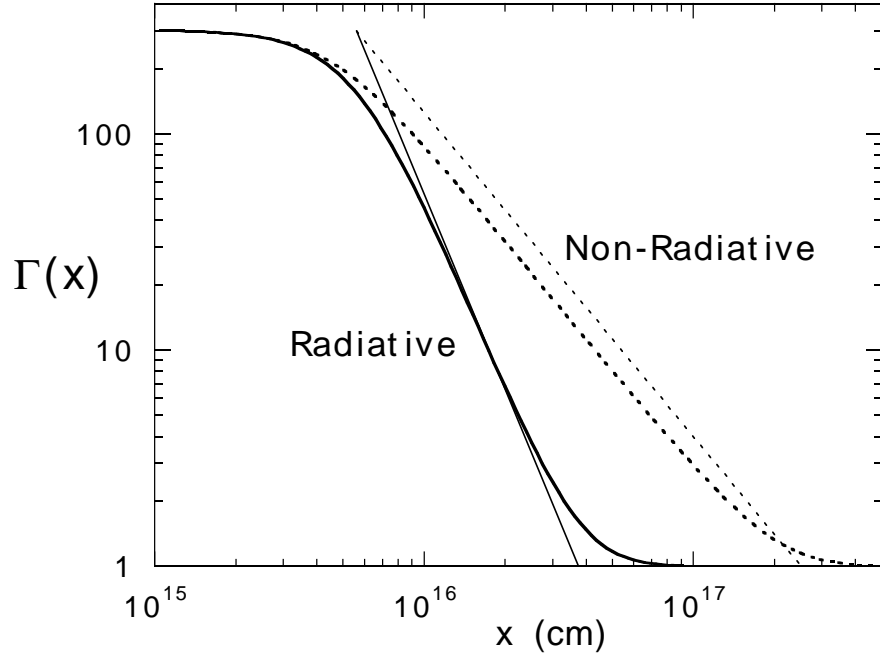
Fig. 2.— Solid and dotted curves show numerical solutions of equation (6) for the plasmoid Lorentz factor Γ as a function of location x in the non-radiative and radiative regimes, respectively. Standard parameter values, shown in Table 1, are used. Solid and dotted lines give the power-law asymptotes in the respective regimes.
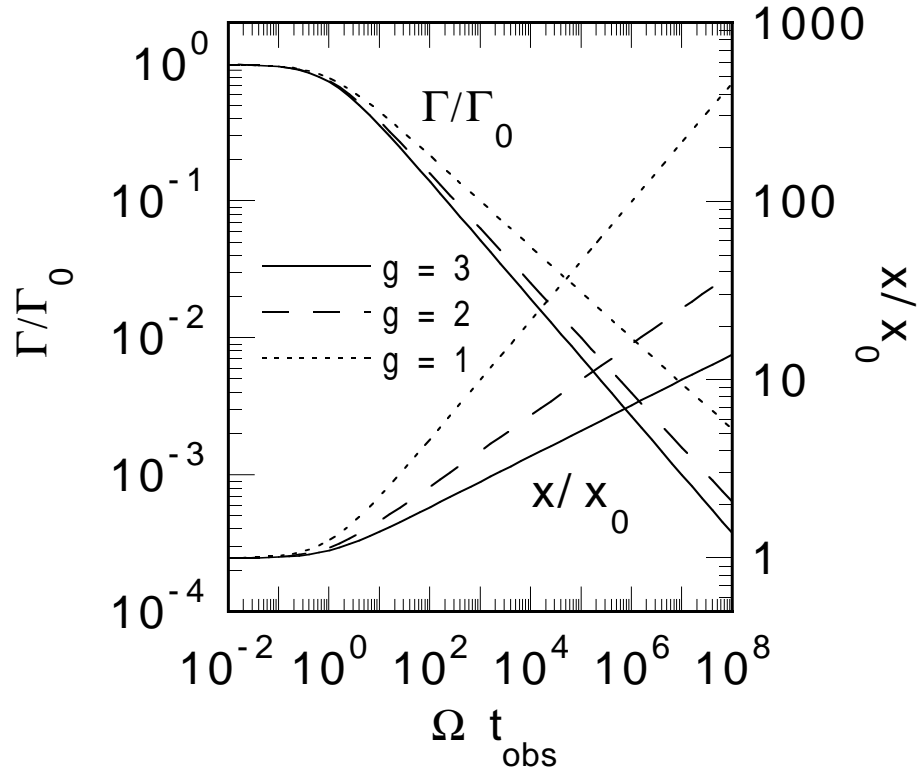
Fig. 3.— Dependence of Γ/Γ_0 amd the ratio of distance traveled to distance x_0 given by equation (15) on the dimensionless quantity Ωt_{obs}, where Ω is given through equation (40) and t_{obs} is the observer time.
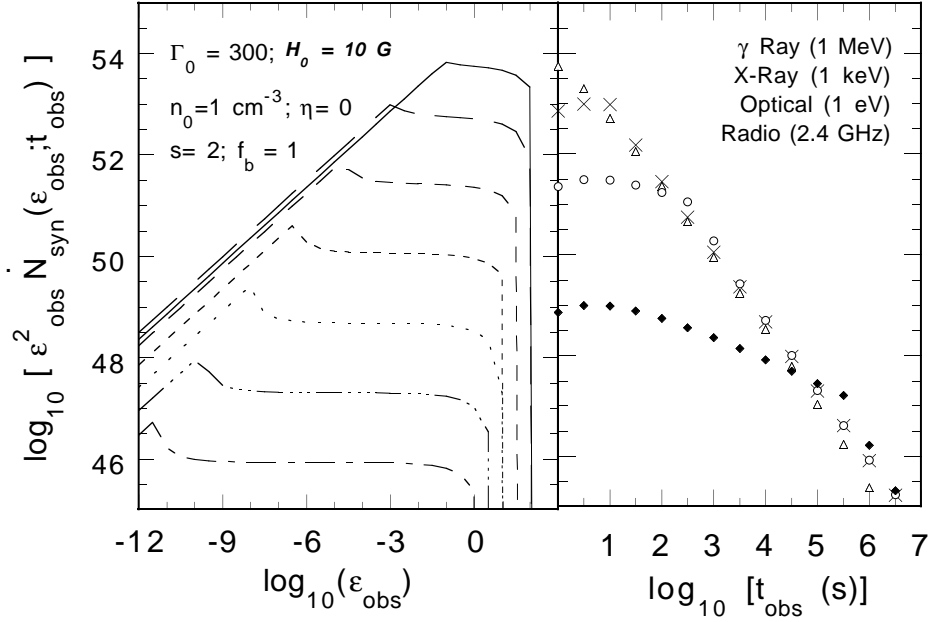
Fig. 4.— Spectra (left) and time profiles (right) of a blast wave decelerating in a uniform external medium. Here it is assumed that the power-law behavior of the blast wave is described by $g = g_r = 3$, and that 100% of the swept-up nonthermal proton energy is transformed into an equally energetic power-law electron distribution with a low-energy cutoff $p_{min} = 0.2$ and a high-energy cutoff $p_{max} = 3 \times 10^6$. All other parameters are standard (see Table 1). Observing times of the spectra are, from top to bottom, 1 sec, 10 sec, 100 sec, etc. The time profiles at 1 MeV, 1 keV, 1 eV, and 2.4 GHz are labeled by triangles, crosses, circles, and filled diamonds, respectively.
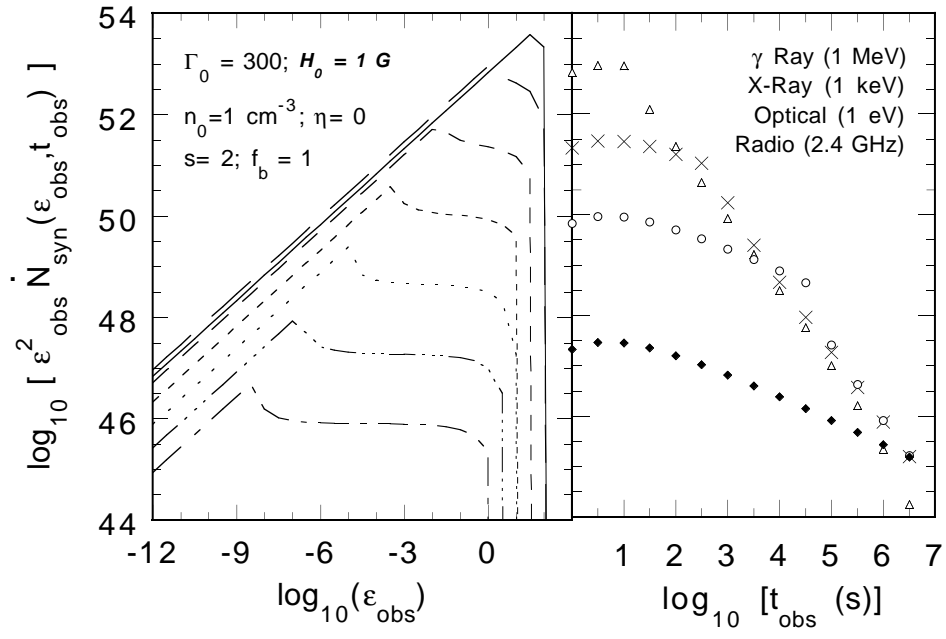
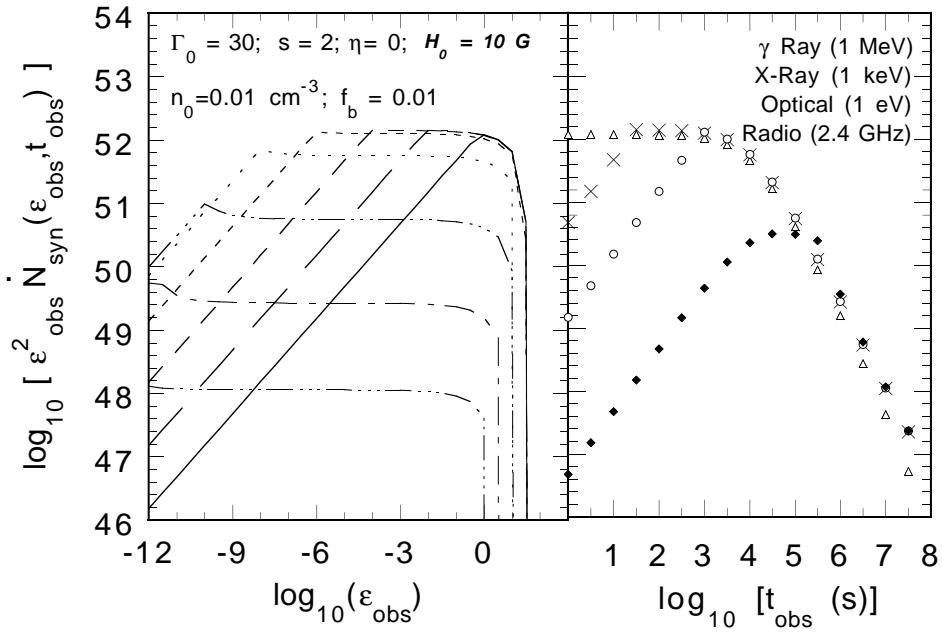Fig. 5.— Same as Fig. 4, except that $H_0 = 1$ Gauss.

Fig. 6.— Same as Fig. 4, except that $\Gamma_0 = 30$, $n_0 = 0.01 \text{ cm}^{-3}$, and $f_b = 0.01$.